GENERATING QUALITY TETRAHEDRAL MESHES FROM BINARY VOLUMES

Mads Fogtmann Hansen, Jakob Andreas Bærentzen and Rasmus Larsen
Department of Informatics and Mathematical Modeling, Technical University of Denmark
Richard Petersens Plads, Blg. 321, Kgs. Lyngby, Denmark

Keywords: Tessellation, Mesh generation, Tetrahedron quality, Signed distance map.

Abstract: This paper presents two new quality measures for tetrahedra which are smooth and well-suited for gradient based optimization. Both measures are formulated as a distance from the regular tetrahedron and utilize the fact that the covariance of the vertices of a regular tetrahedron is isotropic. We use these measures to generate high quality meshes from signed distance maps. This paper also describes an approach for computing (smooth) signed distance maps from binary volumes as volumetric data in many cases originate from segmentation of objects from imaging techniques such as CT, MRI, etc. The mesh generation is split into two stages; a candidate mesh generation stage and a compression stage, where the surface of the candidate mesh is moved to the zero iso-surface of the signed distance maps, while one of the quality measures ensures that the quality remains high.

We apply the mesh generation algorithm on four examples (torus, Stanford dragon, brain mask, and pig back) and report the dihedral angle, aspect ratio and radius-edge ratio. Even though, the algorithm incorporates none of the mentioned quality measures in the compression stage it receives a good score for all these measures. The minimum dihedral angle is in none of the examples smaller than 15^o.

1 INTRODUCTION

High quality tetrahedral mesh generation is an important element in many medical imaging application such as virtual surgery (Suzuki et al., 1998; Kühnapfel et al., 2000; De et al., 2006), image registration (Brock et al., 2005; Montagnat and Delingette, 2005) and biological modeling (McInerney and Terzopoulos, 1996; Cootes et al., 1995). Creation of meshes, which can sustain large soft tissue deformations, is challenging due to high demands in accuracy, efficiency and structural integrity. Efficiency is achieved by having only the minimum required resolution in all areas of the mesh. High resolution is required in high curvature areas near the interface of the object, while lower resolution is sufficient in areas far from the interface and in areas with low curvature. Accuracy and structural integrity are primarily a matter of ensuring that the number of very anisotopic tetrahedra are kept at an absolute minimum. Such tetrahedra will often be biased[1] or/and invert under deformation. Unfortunately, efficiency does not go hand-in-hand with accuracy and structural integrity as anisotopic tetrahedra will emerge when large and small tetrahedra are in close proximity of each other.

In this paper, we propose to generate quality meshes from signed distance maps (SDMs) by generating a candidate mesh as proposed by Molino et al. (Molino et al., 2003) and subsequently compressing the candidate mesh to the surface of the object. The compression is formulated as a gradient based optimization problem where the surface points of the candidate mesh iteratively are moved to zero iso-surface of SDM. A selected quality measure is applied during the compression to regularize the evolution in order to ensure that the quality of the final mesh is high.

An extensive number of quality measures for triangles and tetrahedra can be found in the literature, c.f. (Shewchuk, 2002a; Parthasarathy et al., 1994) for surveys. Most of these measures are non-smooth, only piecewise smooth or difficult to differentiate, and thus not suited for gradient based optimization. Therefore, we propose two new quality measures for tetrahedra which essentially measure the distance or deviation from a given tetrahedron to the regular tetrahedron. They are both differentiable (smooth) and

[1] They exhibit a preferred direction of deformation

Fogtmann Hansen M., Andreas Bærentzen J. and Larsen R. (2009).
GENERATING QUALITY TETRAHEDRAL MESHES FROM BINARY VOLUMES.
In *Proceedings of the Fourth International Conference on Computer Vision Theory and Applications*, pages 5-12
DOI: 10.5220/0001654700050012

rotation- and scale-invariant.

In many of the above mentioned applications the objects to be tesselated are segmented from medical images and therefore represented as binary volumes. We convert a binary volume to a SDM by computing all distances in the volume to the nearest zero-crossing voxel, fitting an implicit function to a suitable narrow band of the zero-crossing distance map and finally computing the distances to the zero iso-surface of the implicit function.

2 RELATED WORK

Early mesh generation in 2D was pioneered with the Delaunay triangulation (Shewchuk, 1996), and it is probably the most widely used technique for 2D mesh generation today. The extension of the Delaunay triangulation to 3D (Weatherhill and Hassan, 1994; Shewchuk, 1998) has unfortunately proven to be unsuitable for many practical application as it admits so-called slivers which are collapsed tetrahedra with a neglilable volume. Several methods for sliver removal (Cheng et al., 2000; Edelsbrunner and Guoy, 2002) have been proposed yet none of these methods have proven to work convincingly (Shewchuk, 1996). Another problem with Delaunay triangulation is that it tessellates the entire convex region of the set of input points, and thus it does not conform to the boundary of the object. Constrained Delaunay methods (Chew, 1989; De Floriani and Puppo, 1992; Shewchuk, 2002b) have been proposed but they are complex and maybe too complex for unstructured mesh generation.

A number of unstructured mesh generation techniques implement a two stage strategy which is similar to our approach . Neugebauer and Klein (Neugebauer and Klein, 1997) use a marching cube mesh as a candidate mesh, Radovitzky and Ortiz (Radovitzky and Ortiz, 2000) use a face-centered cubic lattice, Molino et al. (Molino et al., 2003) use a body-centered cubic (BCC) lattice followed by a subdivision strategy and finally Fuchs (Fuchs, 1997) uses a Delaunay triangulation of vertices placed on a BCC lattice.

In general, two types of strategies have been suggested for the compression: projection and evolution. Neugebauer and Klein (Neugebauer and Klein, 1997) and Grosskopf and Neugebauer (Grosskopf and Neugebauer, 1998) implement projection strategies while Kobbelt et al. (Kobbelt et al., 1999), Wood et al. (Wood et al., 2000) and Molino et al. (Molino et al., 2003) apply evolution strategies using connectivity, spring forces or Laplacian smoothing to regularize the evolution. Molino et al. (Molino et al., 2003) also suggest using aspect ratio (defined as the shortest altitude divided by the longest edge) as a regularizer in a discrete optimization scheme.

3 METHODS

We wish to construct a tetrahedral mesh representation of an object Ω given a signed distance map or binary volume representation of the object. For now we will assume a SDM representation is available and later in this section present an approach for converting a binary volume to a SDM. Formally, we define the Euclidian SDM of an object Ω as a function

$$\Phi(x) = \mathrm{sgn}(x) \min_{y \in \Gamma} \|x - y\|,$$

where

$$\mathrm{sgn}(x) = \begin{cases} -1 & x \in \Omega \\ 1 & x \notin \Omega \end{cases}$$

and Γ is the interface/boundary of the object.

A candidate mesh is generated as described in Molino et al. (Molino et al., 2003). A BCC lattice covering the boundary box of the object is chosen as an initial mesh. Tetrahedra, which are certain to be outside the object, are removed and the resolution of the mesh is increased in the high curvature areas of the SDM of the object using a Red-Green subdivision approach. More tetrahedra are removed in a final step, such that (i) the boundary is a manifold, (ii) no tetrahedra have all four nodes on the boundary, and (iii) no interior edge connects to boundary nodes, c.f. (Molino et al., 2003) for a detailed description. The process is illustrated in Figure 4.

In the compression phase the surface points of the candidate mesh are moved towards the zero iso-surface of the signed distance map (SDM) while a regularizer is applied to ensure a high mesh quality. This is done by minimizing the functional

$$F(\Delta V) = \sum_{1}^{N_s} \Phi(V_{s_i} + \Delta V_{s_i})^2 + \gamma \sum_{i=1}^{N_t} r(V_{T_i} + \Delta V_{T_i}), \quad (1)$$

where V are the vertices of the candidate mesh, ΔV are the displacements of the vertices, s is the set of boundary vertices, T_i contains the id's of the vertices of the ith tetrahedron and r is a regularizer, which measures the quality of a single tetrahedron.

3.1 The Quality of a Tetrahedron

As mentioned, we are interested in generating meshes which are suitable for large deformations, and as such

we wish to define the quality of a tetrahedron in terms of its ability to handle large deformations. In general, if a mesh is biased, such that the tetrahedra are primarily elongated in one direction, the mesh will tend to be either more soft or stiff in the thin direction (Molino et al., 2003). Essentially, the optimal tetrahedron is a regular (equitaterel) tetrahedron. It is however not possible to tessellate a 3D Euclidian space with regular tetrahedra.
Therefore, we wish to describe the quality of a tetrahedron in terms of its distance from a regular tetrahedron. A unique property of a regular tetrahedron is that the covariance matrix of the vertices is isotropic.

Theorem 3.1. *The covariance matrix Σ_T of the vertices of a tetrahedron T is isotropic $\Sigma_T = sI$ iff T is a regular tetrahedron, where s is a scaling factor.*

Proof. Let T be an arbitrary tetrahedron represented by a 3x4 matrix Q containing the four vertices of T. Without loss of generality we will assume that the barycenter of T lie in the origin. Thus, we must prove that

$$\Sigma_T = QQ^T = I, \tag{2}$$

iff T is a regular tetrahedron. s is neglected as it is just a scaling factor.

The regular tetrahedron $\tilde{Q}$ represented by the vertices $(-\frac{1}{\sqrt{2}}, -\frac{1}{\sqrt{12}}, \frac{1}{\sqrt{6}})$, $(\frac{1}{\sqrt{2}}, -\frac{1}{\sqrt{12}}, \frac{1}{\sqrt{6}})$, $(0, \frac{\sqrt{3}}{2}, 0)$ and $(0, -\frac{1}{\sqrt{12}}, -\frac{\sqrt{2}}{\sqrt{3}})$ is a solution to Eq. 2.

For any Q there exists a transformation matrix A such that $Q = A\tilde{Q}$. If Q fulfills Eq. 2 we get

$$QQ^T = A\tilde{Q}\tilde{Q}^T A = AA^T = I.$$

Thus, A is a rotation matrix, which implies that all solutions are geometrically equivalent. It follows that all solutions are regular tetrahedra. □

In contrast to the regular tetrahedron, an elongated tetrahedron has a high variance in the stretched direction and smaller variation perpendicular to that direction. As such an eigenvalue decomposition of the covariance matrix of an elongated tetrahedron will give one eigenvalue (corresponding to the stretched direction) which is relative large compared to the two remaining eigenvalues. The normalized covariance matrix of a regular tetrahedron has eigenvalue 1 with multiplicity 3 (isotropic). This implies that the disparity of the eigenvalues is related to the degree of anisotropicness of a tetrahedron. Inspired by the *Riemannian elastic* (Pennec et al., 2005) and the *St Venant-Kirchoff elastic* (Ciarlet, 1988) energies we propose to use the measures

$$\begin{aligned} r_{log}(V) &= \frac{3}{4}\mathrm{tr}\left(\log^2\left(\frac{\Sigma(V)}{\det(\Sigma(V))^{\frac{1}{3}}}\right)\right) \\ &= \frac{1}{4}\left(3\sum_{i=1}^{3}\log(\lambda_i)^2 - \left(\sum_{i=1}^{3}\log(\lambda_i)\right)^2\right), \end{aligned} \tag{3}$$

and

$$\begin{aligned} r_{eig}(V) &= \frac{1}{4}\mathrm{tr}\left(\left(\frac{\Sigma(V)}{\det(\Sigma(V))^{\frac{1}{3}}} - I\right)^2\right) \\ &= \frac{1}{4}\left(3 + \frac{\sum_{i=1}^{3}\lambda_i^2}{(\prod_{i=1}^{3}\lambda_i)^{\frac{2}{3}}} - 2\frac{\sum_{i=1}^{3}\lambda_i}{(\prod_{i=1}^{3}\lambda_i)^{\frac{1}{3}}}\right), \end{aligned} \tag{4}$$

where $\Sigma(V)$ is the covariance of the vertices V (represented by a 3x4 matrix), λ_i is the ith eigenvalue of covariance matrix Σ and log is the natural logarithm (matrix logarithm when applied to a matrix). The term $\frac{\Sigma}{\det(\Sigma)^{\frac{1}{3}}}$ will be denoted the normalized covariance matrix. The two measures r_{log} and r_{eig} are similar to the above mentioned elastic energies with the exception that the *Cauchy-green* deformation tensor has been replaced by the normalized covariance matrix. Note, that both measures are rotation-invariant as they are based purely on the eigenvalues of the covariance matrix, and scale-invariant as we normalize the covariance matrix. Figure 1 illustrates how the two quality measures behave when a tetrahedron deviates from the regular tetrahedron. A nice property of both measures is that they will evaluate to *infinity* when V describes a collapsed tetrahedron. Furthermore, both quality measures will return zero when applied to a regular tetrahedron.

Given the eigenvalue decomposition $\Sigma = RLR^T$, we can compute the derivative of the measures with respect to Σ by

$$\partial_\Sigma r_{log} = \frac{1}{2}RL^{-1}\left(3\log(L) - I\sum_{i=1}^{3}\log(\lambda_i)\right)R^T.$$

and

$$\begin{aligned} \partial_\Sigma r_{eig} = \frac{1}{2}\Bigg(&\left(\frac{\sum_{i=1}^{3}\lambda_i}{(\prod_{i=1}^{3}\lambda_i)^{\frac{1}{3}}} - \frac{\sum_{i=1}^{3}\lambda_i^2}{(\prod_{i=1}^{3}\lambda_i)^{\frac{2}{3}}}\right)\Sigma^{-1} \\ &- \frac{1}{(\prod_{i=1}^{3}\lambda_i)^{\frac{1}{3}}}I + \frac{1}{(\prod_{i=1}^{3}\lambda_i)^{\frac{2}{3}}}\Sigma\Bigg) \end{aligned}$$

Let P_o denote the projection matrix which centers a tetrahedron such that its barycenter lie in the origin. Hence, $E(V) = VP_oP_o^TV^T$. Thus, the derivatives of the measures with respect to V are

$$\partial_V r_{log} = 2P_oP_o^TV^T\partial_\Sigma r_{log}$$

and

$$\partial_V r_{eig} = 2P_oP_o^TV^T\partial_\Sigma r_{eig}.$$

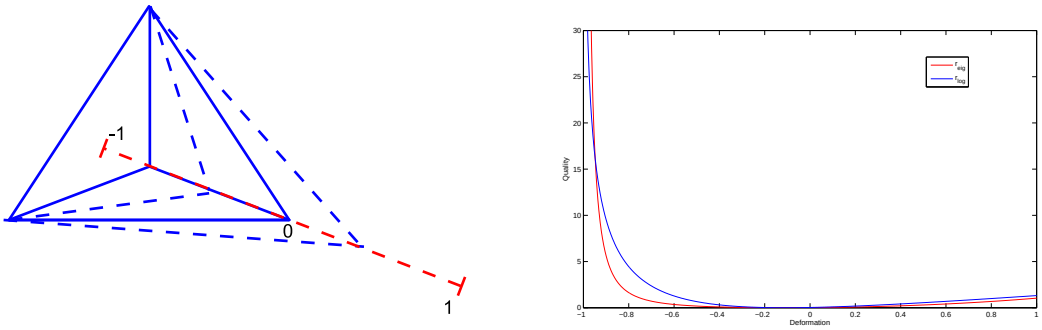

(a) Deformation illustration. (b) Quality as a function of deformation.

Figure 1: Comparison plot of quality measures. Tetrahedra were generated by moving a vertex along the line defined by the normal and the barycenter of the opposite face (regular triangle). The deformation has been scaled such that -1 corresponds to the collapsed tetrahedron and 0 corresponds to the regular tetrahedron.

3.2 Converting a Binary Volume to a Signed Distance Map

A binary volume can be converted to a discretized SDM by computing the Euclidian signed distance $\Phi_{zc}(x)$ from all voxels in the binary volume to the nearest zero-crossing voxel, fitting an implicit surface $I_{srf}(x,w)$ to a suitable narrow band of $\Phi_{zc}(x)$, and finally computing the distances $\tilde{\Phi}(x)$ from all voxels to the zero iso-surface of $I_{srf}(x,w)$.

In this paper, we model the implicit surface $I_{srf}(x,w)$ with a set of cubic B-spline basis functions placed on a regular lattice. The weight parameters w are estimated by minimizing

$$F(w) = \sum_{i=1}^{N} C(x_i,w) + \alpha(\|\nabla I_{srf}(x_i,w)\| - 1)^2, \quad (5)$$

where

$$C(x,w) = \begin{cases} (\Delta d(x,w) - \frac{1}{2}s)^2 & \textbf{if } \Delta d(x,w) > \frac{1}{2}s \\ (\Delta d(x,w) + \frac{1}{2}s)^2 & \textbf{if } \Delta d(x,w) < -\frac{1}{2}s \\ 0 & \textbf{otherwise} \end{cases},$$

$\Delta d(x,w) = \Phi_{zc}(x) - I_{srf}(x,w)$ and s is the width of the voxels. The reason to use $C(x,w)$ as measure of the 'fit' and not the usual *least-squares* fit is that the error of $d_{zc}(x)$ is uniformly distributed. The term $(\|\nabla I_{srf}(x_i,w)\| - 1)$ provides a natural regularization, especially in the zero-crossing areas, as $\|\Phi(x)\| = 1$ is a fundamental property of the Euclidian distance field. The property is not applied as a hard constraint as the B-spline will not be able to fulfill the constraint in the entire narrow band, and the narrow band might contain areas where the true Euclidian distance field is discontinuous.

Given the implicit surface we can find the shortest distance from any voxel x to the zero level set of I_{srf} using the nearest zero-crossing voxel as an initial guess of y. Thus, the task is to find the point y which minimizes $\tilde{\Phi}^2(x,y) = \|x-y\|^2$ s.t. $I_{srf}(y,w) = 0$. This problem can be solved with the Augmented Lagrangian method (Madsen et al., 2004). Alternatively, y can be updated iteratively with $-\tau dy$, where dy is given by

$$dy = \nabla I_{srf}(y,w) I_{srf}(y,w) + \beta(I - nn^T)(x-y), \quad (6)$$

and $n = \frac{\nabla I_{srf}(y,w)}{\|I_{srf}(y,w)\|}$ is normal of the iso-surface at the point y. The first term of dy pushes the point y towards the zero iso-surface, while the second term tries to minimize the distance between x and y by moving y in the tangential plane of the surface. A suitable τ can be found with line-search. Selecting $\beta = 0.1$ seems to work in most cases.

4 IMPLEMENTATION ISSUES

If Eq. 1 is differentiable it can be minimized by a gradient based optimization scheme. As the discrete representation of the SDM is obviously not differentiable we wrap the SDM with a cubic B-spline interpolator such that the signed distances and derivatives can be evaluated in the entire Euclidean space. Furthermore, as the regularization term in Eq. 1 works independently on each tetrahedron it does not directly discourage overlap between the tetrahedra in a mesh. We handle this issue by having the regularizer return *infinity* if an invertion/overlap occurs. This is theoretically correct as our measures evaluate to *infinity* in the case of a collapsed tetrahedron - in an evolution based approach a tetrahedron must collapse before it can invert. We minimize Eg. 1 using a limited memory BFGS optimizer.

5 RESULTS

To test the quality measures, we have selected four examples. The first example is the torus where the SDM was computed directly from the parametrization of the torus. The second example is the Stanford dragon where the SDM was computed from the polygonal mesh. The third example is a brain mask which was extracted from a MRI of a human brain. The final example is a half pig back which was extracted from a CT scan by thresholding the background. The SDMs of the two last examples were computed as described in Section 3.2.

The resulting tetrahedral meshes are displayed in Figures 2, 3, 4 and 5. The meshes shown in the figures were generated with r_{eig}. Tables 1 and 2 list the minimum and maximum dihedral angles (MiDA and MaDA), the maximum and average aspect ratio (MaAR and AvAR) as well as the maximum and average radius-edge[2] ratio (MaRE and AvRe) for r_{log} and r_{eig}, respectively. From Tables 1 and 2 we note that r_{eig} in general obtain slightly better results than r_{log}.

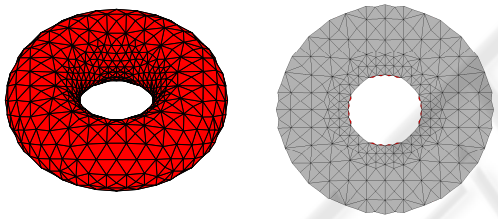

(a) Full (b) Sliced

Figure 2: Tetrahedral mesh of torus.

Molino et al. (Molino et al., 2003) report the MiDA, MaDA MaAR and AvAR for a tetrahedral mesh of the Stanford dragon consisting of approximately 500k elements (comparable to our dragon mesh) as shown in Table 3. In the case of the Stanford dragon our measures r_{log} and r_{eig} obtain better scores for MiDA and AvAR and a worse score for MaDa than the two approaches in Molino et al. Futhermore, Molino et al. are only able to obtain a lower MaAR when minimizing the aspect ratio. It should be noted that our approach regardless of the quality measure is able to obtain a lower AvAR than Molino et al., even though they use the aspect ratio as an regularizer. The elastic regularizer reported in Molino et al. is likewise able to obtain a better AvAR which indicates that the applied optimization procedure fails to produce the optimal result.

[2]Radius of circum-cycle over the minimum edge length

Table 1: Quality of generated meshes using r_{log}.

	Torus	Dragon	Brain	Carcass
MiDA	36^o	19^0	26^o	15^o
MaDA	144^o	157^0	146^o	165^o
MaRE	1.1	2.3	1.5	2.2
AvRE	0.7	0.8	0.8	0.8
MaAR	3.3	6.7	4.4	7.9
AvAR	1.8	1.9	1.8	2.1

Table 2: Quality of generated meshes using r_{eig}.

	Torus	Dragon	Brain	Carcass
MiDA	36^o	19^o	27^o	16^o
MaDA	144^o	159^o	144^o	163^o
MaRE	1.1	2.4	1.3	2.3
AvRE	0.8	0.8	0.8	0.8
MaAR	3.1	6.4	3.9	7.9
AvAR	1.8	1.9	1.8	2.0

Table 3: Quality of dragon mesh (500K elements) reported in (Molino et al., 2003). Two different regularizers were applied in the compression phase; one which uses elastic springs and one which tries to minimize the aspect ratio.

	Elastic regularizer	Aspect ratio
MiDA	13^o	16^o
MaDA	154^o	150^o
MaAR	7.6	5.3
AvAR	2.2	2.3

6 DISCUSSION

We have proposed two new quality measures and tested them on four examples. In section 5 Results we compared our results for the Stanford dragon with the results presented in (Molino et al., 2003). It should be stated that comparison may not be fair, as we have not used the same SDM or candidate mesh as Molino et al (Molino et al., 2003). Our final dragon mesh is visually close to identical with the dragon mesh in (Molino et al., 2003), and the numbers of the tetrahedra in the two meshes are comparable. Thus, we believe that the comparison is quite fair. In the future, we will test the proposed measures in different applications and develop them further. E.g. it is possible to incorporate a weighting matrix into the quadratic form of the measures allowing for preferred directions of deviation from the regular tetrahedron

$$r_W(V) = \frac{3}{4}\mathrm{tr}\left(\log\left(\frac{\Sigma(V)}{\det(\Sigma(V))^{\frac{1}{3}}}\right) W \log\left(\frac{\Sigma(V)}{\det(\Sigma(V))^{\frac{1}{3}}}\right)\right)$$

and to normalize the covariance matrix with its trace (sum of eigenvalues) instead of its determinant (product of eigenvalues)

$$r_{tr}(V) = \frac{3}{4}\mathrm{tr}\left(\log^2\left(3\frac{\Sigma(V)}{\mathrm{tr}(\Sigma(V))}\right)\right).$$

REFERENCES

Brock, K., Sharpe, M., Dawson, L., Kim, S., and Jaffray, D. (2005). Accuracy of finite element model-based multi-organ deformable image registration. *Medical Physics*, 32:1647.

Cheng, S., Dey, T., Edelsbrunner, H., Facello, M., and Teng, S. (2000). Silver exudation. *Journal of the ACM (JACM)*, 47(5):883–904.

Chew, L. (1989). Constrained Delaunay Triangulations. *Algorithmica*, 4(1):97–108.

Ciarlet, P. (1988). Mathematical Elasticity, Vol. I. *Studies in Mathematics and its Applications*, 20.

Cootes, T., Taylor, C., Cooper, D., Graham, J., et al. (1995). Active Shape Models-Their Training and Application. *Computer Vision and Image Understanding*, 61(1):38–59.

De, S., Lim, Y., Manivannan, M., and Srinivasan, M. (2006). Physically Realistic Virtual Surgery Using the Point-Associated Finite Field (PAFF) Approach. *PRESENCE: Teleoperators and Virtual Environments*, 15(3):294–308.

De Floriani, L. and Puppo, E. (1992). An on-line algorithm for constrained Delaunay triangulation. *CVGIP: Graphical Models and Image Processing*, 54(4):290–300.

Edelsbrunner, H. and Guoy, D. (2002). An Experimental Study of Sliver Exudation. *Engineering with Computers*, 18:229–240.

Fuchs, A. (1997). *Automatic Grid Generation with Almost Regular Delaunay Tetrahedra*. SFB 404, Geschäftsstelle.

Grosskopf, S. and Neugebauer, P. (1998). Fitting geometrical deformable models to registered range images. *Lecture notes in computer science*, pages 266–274.

Kobbelt, L., Vorsatz, J., Labsik, U., and Seidel, H. (1999). A Shrink Wrapping Approach to Remeshing Polygonal Surfaces. *Computer Graphics Forum*, 18(3):119–130.

Kühnapfel, U., Çakmak, H., and Maaß, H. (2000). Endoscopic surgery training using virtual reality and deformable tissue simulation. *Computers & Graphics*, 24(5):671–682.

Madsen, K., Nielsen, H., and Tingleff, O. (2004). A comparison of tetrahedron quality measures. Technical report, Technical university of Denmark.

McInerney, T. and Terzopoulos, D. (1996). Deformable models in medical image analysis: a survey. *Medical Image Analysis*, 1(2):91–108.

Molino, N., Bridson, R., Teran, J., and Fedkiw, R. (2003). A crystalline, red green strategy for meshing highly deformable objects with tetrahedra. In *In 12th Int. Meshing Roundtable*, pages 103–114.

Montagnat, J. and Delingette, H. (2005). 4D deformable models with temporal constraints: application to 4D cardiac image segmentation. *Medical Image Analysis*, 9(1):87–100.

Neugebauer, P. and Klein, K. (1997). Adaptive triangulation of objects reconstructed from multiple range images. *IEEE Visualization97, Late Breaking Hot Topics*.

Parthasarathy, V., Graichen, C., and Hathaway, A. (1994). A comparison of tetrahedron quality measures. *Finite Elements in Analysis and Design*, 15(3):255–261.

Pennec, X., Stefanescu, R., Arsigny, V., Fillard, P., and Ayache, N. (2005). Riemannian Elasticity: A Statistical Regularization Framework for Non-linear Registration. *LECTURE NOTES IN COMPUTER SCIENCE*, 3750:943.

Radovitzky, R. and Ortiz, M. (2000). Tetrahedral mesh generation based on node insertion in crystal lattice arrangements and advancing-front-Delaunay triangulation. *Computer Methods in Applied Mechanics and Engineering*, 187(3-4):543–569.

Shewchuk, J. (1996). Triangle: Engineering a 2D Quality Mesh Generator and Delaunay Triangulator. *Lecture Notes In Computer Science; Vol. 1148*, pages 203–222.

Shewchuk, J. (1998). Tetrahedral mesh generation by Delaunay refinement. *Proceedings of the fourteenth annual symposium on Computational geometry*, pages 86–95.

Shewchuk, J. (2002a). A comparison of tetrahedron quality measures. Technical report, University of California at Berkeley.

Shewchuk, J. (2002b). Constrained Delaunay Tetrahedralizations and Provably Good Boundary Recovery. *Proceedings of the 11th International Meshing Roundtable*, pages 193–204.

Suzuki, N., Hattori, A., Ezumi, T., Uchiyama, A., Kumano, T., Ikemoto, A., Adachi, Y., and Takatsu, A. (1998). Simulator for virtual surgery using deformable organ models and force feedback system. *Stud Health Technol Inform*, 50:227–33.

Weatherhill, N. and Hassan, O. (1994). Efficient three-dimensional Delaunay triangulation with automatic point creation and imposd boundary constraints. *International journal for numerical methods in engineering*, 37(12):2005–2039.

Wood, Z., Schroder, P., Breen, D., and Desbrun, M. (2000). Semi-regular mesh extraction from volumes. *IEEE Visualization: Proceedings of the conference on Visualization'00*, 2000:275–282.

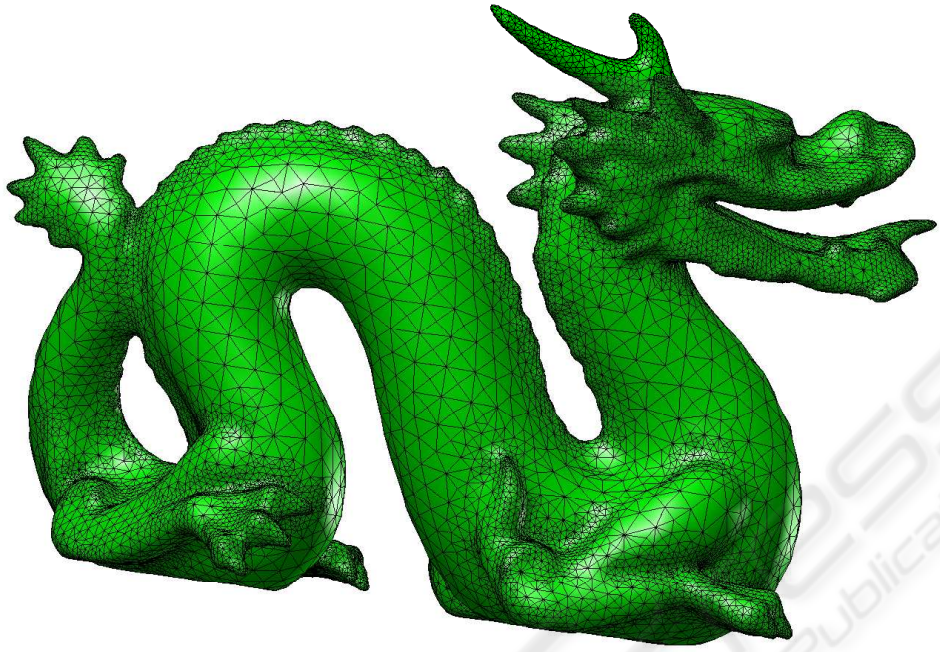

Figure 3: Tetrahedral mesh of dragon (540K elements).

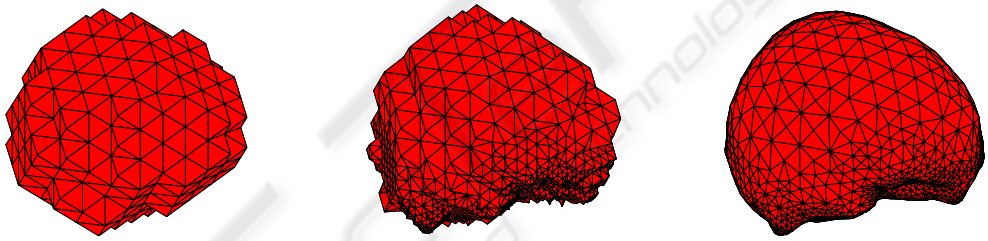

(a) Initial (b) Candidate (c) Final

Figure 4: Tetrahedral mesh from mask of human brain (80K elements).

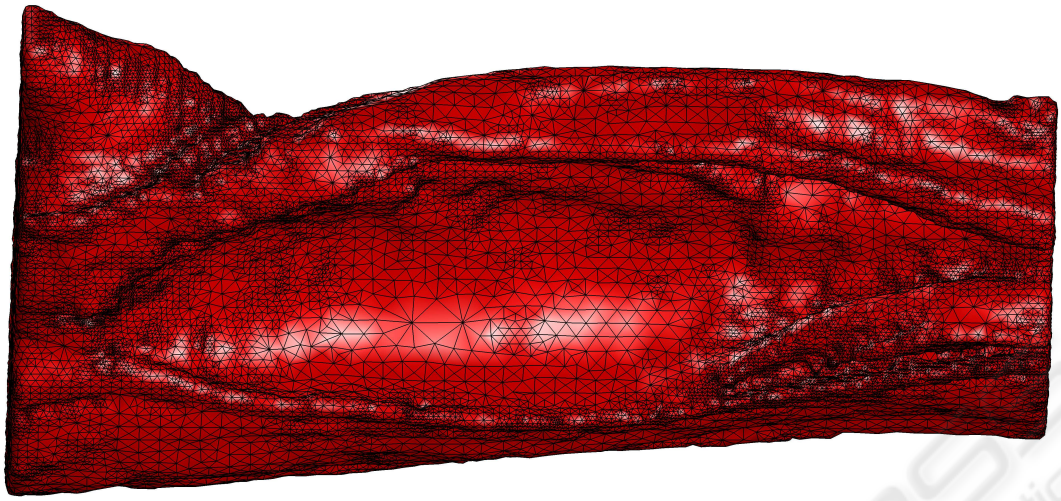

Figure 5: Tetrahedral mesh of half pig back (280k elements).